ISSN1027-5495. Functional Materials, 31, No.2 (2024), p. 153-162
doi:http://dx.doi.org/10.15407/fm31.02.153

Preparation and characterization of ^{6}LiF/ZnS(Ag) scintillator with varying granulometry

V. Tarasov[1], O. Zelenskaya[1], O. Shpilinskaja[2], L. Trefilova[3], L. Andruschenko[3], L. Borysova[3], Yu. Hapon[3]

[1]Institute for Scintillation Materials of NASU, 60, Nauky Avenue, Kharkiv, Ukraine, 61023
[2]National Aerospace University «Kharkiv Aviation Institute», 17, Chkalov str., Kharkiv, Ukraine, 61070
[3]National University of Civil Protection of Ukraine, 94, Chernyshevska str., Kharkiv, Ukraine, 61023

Received August 23, 2023

The effect of the dispersity of ^{6}LiF and ZnS(Ag) powders on the performance of a ^{6}LiF/ZnS(Ag) composite scintillator with a mass ratio of ^{6}LiF/ZnS(Ag)/binder component mass ratio of 1 ^{6}LiF:4ZnS(Ag):2.1 binder was studied. It has been established that for a single-layer ^{6}LiF/Zn S(Ag) composite with a thickness of 0.2 mm, the best light output and thermal neutron detection efficiency (~29%) is provided at ratios of 1 to (10.3-13.3) for ^{6}LiF and ZnS(Ag) grain size and (550-1150) to 1 for their number of grains respectively. Outside these optimal ratios, the detection efficiency drops to 20-22%. When the ratio of the number of the ^{6}LiF and ZnS(Ag) grains is below optimal, the detection efficiency decreases due to a decrease in the probability of neutron capture by a reduced number of ^{6}Li nuclei. A significant excess of ^{6}LiF increases both the neutron capture probability and the absorption probability of the charged products of the neutron capture reaction in the same ^{6}LiF converter, without causing scintillations in ZnS(Ag). It has been shown that a scintillation detector constructed from five ^{6}LiF/ZnS(Ag) layers, alternating with four organic glass plates acting as light guides ensures a thermal neutron detection efficiency of 75%.

Keywords: neutron detector, ^{6}LiF/ZnS(Ag), converter, scintillator, detection efficiency, light yield

Отримання та характеризація ^{6}LiF/ZnS(Ag) сцинтилятора різної гранулометрії.
В. Тарасов, О. Зеленська, О. Шпилинська, Л. Трефілова, Л. Андрющенко, Л. Борисова, Ю. Гапон

Досліджено вплив дисперсності порошків ^{6}LiF і ZnS(Ag) на робочі характеристики композиту ^{6}LiF/ZnS(Ag) з масовим співвідношенням компонентів 1 ^{6}LiF:4 ZnS(Ag):2,1 (сполучна речовина). Встановлені співвідношення розмірів від 1 до (10,3÷13,3) і числа від (550÷1150) до 1 зерен конвертера ^{6}LiF до розмірів і кількості зерен сцинтилятора ZnS(Ag), які забезпечують кращі значення світлового виходу та ефективності реєстрації теплових нейтронів (~ 29 %) для одношарового композитного сцинтилятора ^{6}LiF/ZnS(Ag) товщиною 0,2 мм. За межами цього діапазону ефективність реєстрації знижується до 20-22%. При співвідношенні кількості зерен ^{6}LiF і ZnS(Ag) нижче оптимальної, ефективність детектування знижується через зменшення ймовірності захоплення нейтронів зменшеною кількістю ядер ^{6}Li. Значний надлишок ^{6}LiF збільшує як ймовірність захоплення нейтронів, так і ймовірність поглинання заряджених продуктів реакції захоплення нейтронів у тому ж самому конвертері ^{6}LiF без виникнення сцинтиляцій у ZnS (Ag). Показано, що конструкція сцинтиляційного детектора, яка складається з п'яти шарів ^{6}LiF/ZnS (Ag), розділених чотирма пластинами з органічного скла, що виконують роль світловодів, забезпечує ефективність реєстрації теплових нейтронів, що становить 75%.

1. Introduction

It is well known [1] that gas discharge tubes filled with inert gas ^{3}He are highly efficient neutron detectors (especially in the thermal energy region) with low sensitivity to γ-radiation, low inherent background, high spatial resolution as well as the stability of performance over time. The production of ^{3}He detectors for national security, nuclear security [2,3] and neutron scattering applications [4-7] is hampered by the problem of a shortage of the ^{3}He isotope due to its extremely low natural abundance (~ 10^{-4} %) in natural helium.

Solid-state scintillators are a suitable alternative to the ^{3}He gas-discharge tubes for thermal neutron detection [1,2,7-9]. They are homogeneous or heterogeneous materials containing isotopes with a high neutron capture cross-section. Such isotopes called "converters" capture incoming neutrons and transform them into charged particles and/or γ-quanta. This secondary radiation interacts with the electron sub-system of the scintillation material causing flashes of light (scintillations) that can be detected and quantified.

The choice of the neutron radiation converter largely determines the detection efficiency, spatial and energy resolution of the thermal neutron detector. The most suitable converters for thermal neutrons are the ^{6}Li and ^{10}B isotopes with large capture cross-sections 940 and 3840 barns, respectively [1, 8]. ^{6}Li converts the captured neutron into a triton (^3_1H) and an α-particle (^4_2He) with energies of 2.73 and 2.05 MeV, respectively:

$$^6_3Li + ^1_0n \rightarrow ^3_1H + ^4_2\alpha + 4.78\,MeV, \qquad (1)$$

The reaction of neutron capture by the ^{10}B follows through two channels:

$$^{10}_5B + ^1_0n \rightarrow ^7_3Li^* + ^4_2\alpha + 2.792\,MeV$$
(the ground state; 6% branching ratio)
$$^{10}_5B + ^1_0n \rightarrow ^7_3Li^* + ^4_2\alpha + 2.310\,MeV$$
(the exited state; 94% branching ratio) (2)

In the first channel, ^{10}B decays into ^{7}Li in the ground state and an α-particle with energy of 1.0 MeV and 1.792 MeV, respectively. In the second channel, ^{10}B decays into ^{7}Li in an excited state (^{7}Li*) and an α-particle with energies of 0.84 MeV and 1.47 MeV, respectively. ^{7}Li* appears in 94% of cases, and its transition to the ground state is accompanied by the emission of a γ-quantum with an energy of 480 keV.

According to [8], the absorption length of thermal neutrons in chemical compounds containing Li and B elements enriched in ^{6}Li and ^{10}B isotopes is 1 mm and 0.1 mm, respectively. However, although the ^{10}B nuclei capture neutrons four times more efficiently than the ^{6}Li ones, the reaction products of neutron capture by ^{6}Li have higher energy and do not contain γ-quanta, which provides better discrimination of neutrons/gamma radiation at the relatively high background of γ-radiation [10]. Thus, in principle, the ^{6}Li nucleus is the best converter of a thermal neutron into charged particles (α and triton), whose energy is converted by a scintillator into flashes of light. Due to the high chemical activity of lithium, ^{6}LiF salt is the preferred choice as a converter since it is chemically stable [11].

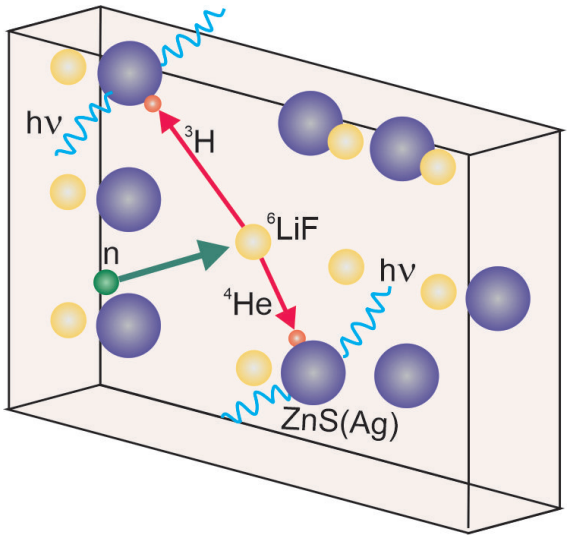

Fig. 1. Thermal neutron detection scheme in ^{6}LiF/ZnS(Ag).

ZnS(Ag) is a highly efficient scintillator used widely to detect α- and other short-range radiation [12]. This scintillation material is resistant to corrosive and humid atmospheres. Among all scintillators, ZnS(Ag) has the highest absolute light yield of 95,000 photons per 1 MeV [13,14]. When ZnS(Ag) is admixed with ^{6}LiF, it provides a high scintillation response to thermal neutrons (160,000 photons per neutron) [10,15]. However, ZnS(Ag) is available only in powder form [16], consisting of multiple crystalline grains randomly positioned. Due to the re-absorption and scattering of the light emitted by ZnS(Ag) under irradiation, there is a significant difference between its absolute and technical light yield. Poor light collection causes this difference [10,13].

Fig. 1 schematically shows the process of detecting thermal neutrons in the ^{6}LiF/ZnS(Ag) composite material; it is a powder mixture of

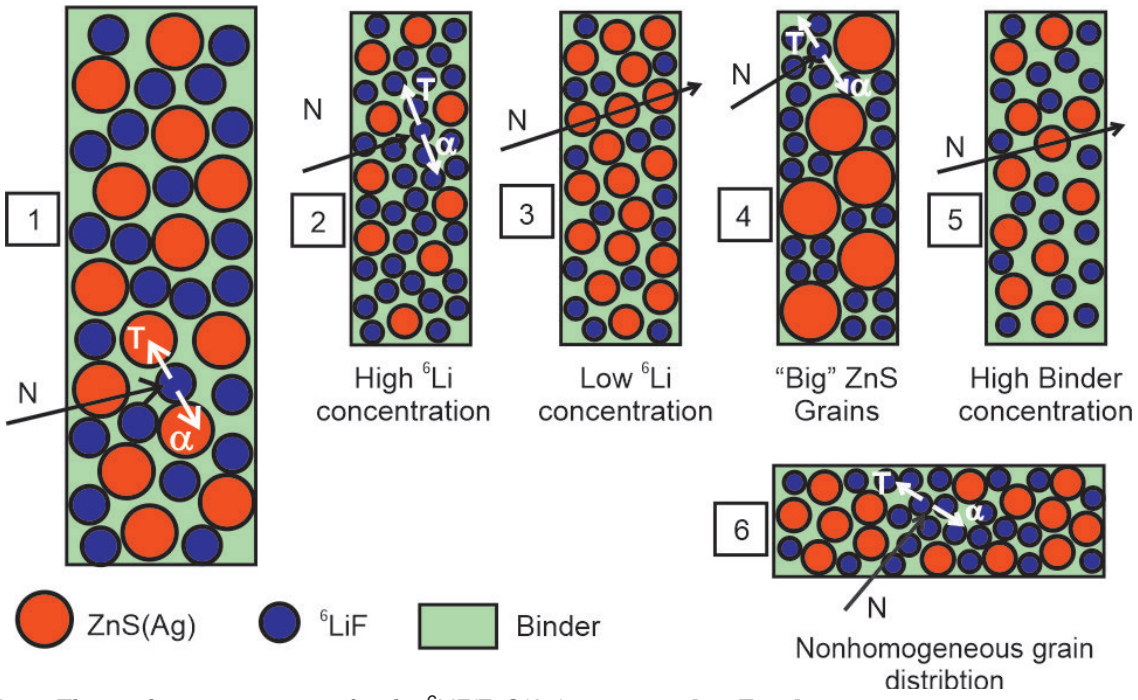

Fig. 2 The configuration options for the ^{6}LiF/ZnS(Ag) composite [24, Fig.5].

^{6}LiF converter and ZnS(Ag) scintillator, bonded with a binder such as polyethylene, plastic, epoxy, sodium silicate, or other suitable material [6,17,18]. Note that the energy loss of the reaction products of the neutron capture in the binder is usually insignificant.

The scintillation process in ZnS(Ag) is due to the recombination of spatially separated donor-acceptor pairs responsible for the luminescence band peaking at λ_{max} = 450 nm (E_{ph}=2.8 eV) [19,20]. ZnS(Ag) responds differently to γ-, β- and α-radiation [21]. The light yield per 1 MeV of the absorbed energy of β-particles or γ-quanta is about 2–5% of that of α-particles. Such a difference in the light yield of α- and β- or γ-radiation is exploited for discrimination of ionizing radiation. A certain detection threshold when analyzing the amplitude of a scintillation pulse, makes it possible to isolate high-amplitude signals caused by α-particles and filter out low-amplitude signals related to β- or γ- radiation. When detecting thermal neutrons, the contribution of γ-quanta to the scintillation response of ^{6}LiF/ZnS(Ag) does not exceed 10^{-6} [10, 22]; this makes this composite material preferable when it is necessary to discriminate neutron and gamma radiation.

According to [23], the non-exponential decay of luminescence is a characteristic feature of the donor-acceptor recombination mechanism. The sum of two exponential components and one hyperbolic component with time constants 26 ns, 130 ns, and 1.1 μs describes to the luminescence decay kinetics of ZnS(Ag) [19]. The scintillation decay time τ_d is estimated at 110-113 ns, which is the time of decrease in the luminescence intensity of ZnS(Ag) by e times. Compared to other scintillators, ZnS(Ag) responds quickly to γ-rays and β-particles and slowly to α-particles. In ^{6}LiF/ZnS(Ag), gamma-quantum detection events take about 90 ns, while neutron detection events typically last more than 200 ns [24]. Therefore, the ^{6}LiF/ZnS(Ag) composite is the most appropriate scintillator to detect thermal neutrons due to discrimination by the shape of the scintillation pulse.

The light yield, registration efficiency and spatial resolution of ^{6}LiF/ZnS(Ag) composite depend significantly on the powder dispersity, the proportion of components in the mixture ^{6}LiF/ZnS(Ag)+binder and the type of binder used [6,25,26]. The concentration of ^{6}LiF determines how many neutrons it will absorb to convert them into charged particles. However, not all of them will cause scintillations; to do this they need to penetrate into the ZnS(Ag) grains. The ZnS(Ag) concentration determines this probability and the total probability of scintillation emission by the ^{6}LiF/ZnS(Ag) composite after neutron absorption.

The authors of [24] considered the configuration options for the ^{6}LiF/ZnS(Ag) composite (Fig. 2) to characterize each of them as follows:

1. Under certain conditions, an optimal configuration is obtained, in which the neutron capture reaction products ionize ZnS(Ag) grains to form scintillations.

2. Excess lithium increases the probability of neutron capture but causes a few scintillations.

3. Lithium deficiency reduces the probability of neutron capture.

4. Too large ZnS grains and, consequently, large cavities between them lead to a decrease in the probability of neutron capture reaction products entering ZnS(Ag) grains.

5. Binder excess reduces the probability of neutron capture.

6. Non-uniform distribution of the ZnS(Ag) grains (clustering) gives the same effect as an increase in the size of these grains.

Thus, there should be an optimal ratio between the ^{6}LiF and ZnS(Ag) concentrations, which also depends on the thickness of the ^{6}LiF/ZnS(Ag) layer scattering light. The transparency of this opaque composite can be improved by increasing the binder concentration [26]. According to literature data, the most promising mixtures are 1^{6}LiF):5 (ZnS(Ag):1 binder with the thickness 0.65 mm [18], 1^{6}LiF:3ZnS(Ag):1 binder with the thickness 0.22 mm [15]; 1^{6}LiF:2 ZnS(Ag):1 (binder) with the thickness 0.8 mm [17,25] and 1^{6}LiF:3 ZnS(Ag):0.6 binder with the thickness 1.35 mm, using a spectrum-shifting fiber [24].

The grain size of the ^{6}LiF and ZnS(Ag) powders also significantly affects the efficiency of converting thermal neutrons into optical photons. When the grain size of the ^{6}LiF powder exceeds the range of α-particles, they will not be able to leave the converter and reach ZnS(Ag); therefore, the conversion efficiency of the ^{6}LiF/ZnS(Ag) composite will decrease. At the same time, the grain size of the ZnS(Ag) powder must be large enough to absorb most of the energy of the α-particle and triton.

Table 1 shows the ranges of the α-particle and triton in the ^{6}LiF converter and ZnS(Ag) scintillator, according to the calculations of various authors [6,26,27-29]. A comparative analysis of the data in Table 1 leads to the conclusion that the ranges of the α-particle and the triton in ZnS(Ag) are within 4.79 -7 μm and 22-32 μm, respectively, and their ranges in ^{6}LiF cover approximately the same distances as in ZnS(Ag).

To obtain the ^{6}LiF/ZnS(Ag) composite with improved performance, it is necessary to optimize the grain size of the converter and scintillator so that the grains of the ^{6}LiF powder would be significantly smaller than the grains of the ZnS(Ag) powder. According to [29], for an ultrathin thermal neutron detector consisting of ZnS(Ag) and ^{6}LiF layers successively deposited in vacuum, the maximum count rate is achieved at a thickness of 15 and 6 μm, respectively. It follows that the optimal thickness of the ZnS(Ag) layer is approximately half as long as the triton range. Thus, in the optimal ZnS(Ag) layer, alpha particles, compared to tritons, lose much more energy, which is then converted into optical photons. Increasing the thickness of this layer will certainly enhance luminescence yield due to increasing the energy loss of tritons, however, it will worsen the light transport and, consequently, the performance of the ^{6}LiF/ZnS(Ag) detector. Thus, the scintillation response of the ^{6}LiF/ZnS(Ag) composite to thermal neutrons depends mainly on the interaction of ZnS(Ag) with alpha particles rather than tritons.

Monte Carlo simulation established, that with an increase in the mass fraction of ZnS(Ag), the light yield of the ^{6}LiF/ZnS(Ag) composite reaches its maximum at a larger ZnS(Ag) grain size [6]. In particular, the highest light yield of ^{6}LiF/ZnS(Ag) with ZnS(Ag) grain size of 10 μm is obtained at the mass ratio of 1^{6}LiF):2 ZnS(Ag). GEANT4 simulation of the light yield for a mixture with the component mass ratio of 1 ^{6}LiF:2 (ZnS(Ag):0.3 (binder) and with different ZnS(Ag) grain size (1, 2, 4, 8, and 16 μm) has demonstrated that for smaller grain sizes, the scintillation response per neutron capture event is more uniform [24]. Note that the simulation of the operating parameters of a composite does not consider real powders with grains of different sizes. The difference in grain sizes is taken into account by its granulometry, that is, the distribution of the number of grains by size with a maximum corresponding to the average grain size (for example, the average diameter).

This work aims to establish the effect of the average grain size of the ^{6}LiF and ZnS(Ag) powders on the light yield and the detection efficiency of the thermal neutron detector based on ^{6}LiF/ZnS(Ag).

Table 1. Ranges of the $^{6}Li(n,\alpha)^{3}H$ nuclear reaction products.

Range of the α-particle with energy 2.05 eV, (μm)		Range of the triton ^{3}H with energy 2.73 eV, (μm)		References
^{6}LiF	ZnS(Ag)	^{6}LiF	ZnS(Ag)	
5.08	4.79	28.1	27.2	[6]
8.3	8.6	22.0	22.4	[27]
7	7	32	32	[26]
6		32		[28]
4	6	20	32	[29]

2. Experimental

Powders fractions of various dispersion were obtained by dynamic sedimentation of commercial ^{6}LiF and ZnS(Ag) powders in a centrifuge with the addition of a surfactant. The granulometry of the powder fractions was analyzed using an LMS-30 laser microanalyzer; the average grain size was determined, corresponding to the maximum on the distribution curve of the number of grains depending on their size.

Samples of the $^{6}LiF/ZnS(Ag)$ composite were obtained by dispersing a mixture of ^{6}LiF and ZnS(Ag) powder fractions in XTR-311 optical epoxy adhesive produced by His Glassworks, Inc (USA). The adhesive is a two-component mixture that hardens at room temperature at the mass ratio of its components of 10:3. The composite samples with the component mass ratio of 1 ^{6}LiF:4 ZnS(Ag):2.1 (binder) were obtained by squeegee spreading the mixture onto organic glass plates measuring 40×25×3 mm^3 to form a layer with a thickness of 0.2 mm.

Pulse-height spectra of the obtained samples $^{6}LiF/ZnS(Ag)$ were measured by an experimental setup consisting of a charge-sensitive preamplifier BUS 2-94, amplifier BUS 2-95, and a multichannel analyzer AMA03-F. A sample $^{6}LiF/ZnS(Ag)$ was mounted on the input window of a Hamamatsu R1307 photomultiplier tube with an optical contact.

The radiation sources employed were a 5.5 MeV α-particle source ^{241}Am and a certified neutron source ^{239}Pu-Be with neutron yield equal to $1{\cdot}10^{5}$ neutrons per second.

The relative light yield of the obtained $^{6}LiF/ZnS(Ag)$ samples was estimated by the position of the maxima in the pulse-height spectrum measured under α-irradiation from a ^{241}Am source.

To produce thermal neutrons, a ^{239}Pu-Be neutron source was placed in a polyethylene spherical moderator with a certified thermalization coefficient of 10%. A 1 mm thick screen made of metallic cadmium with a natural isotopic composition was used to determine the

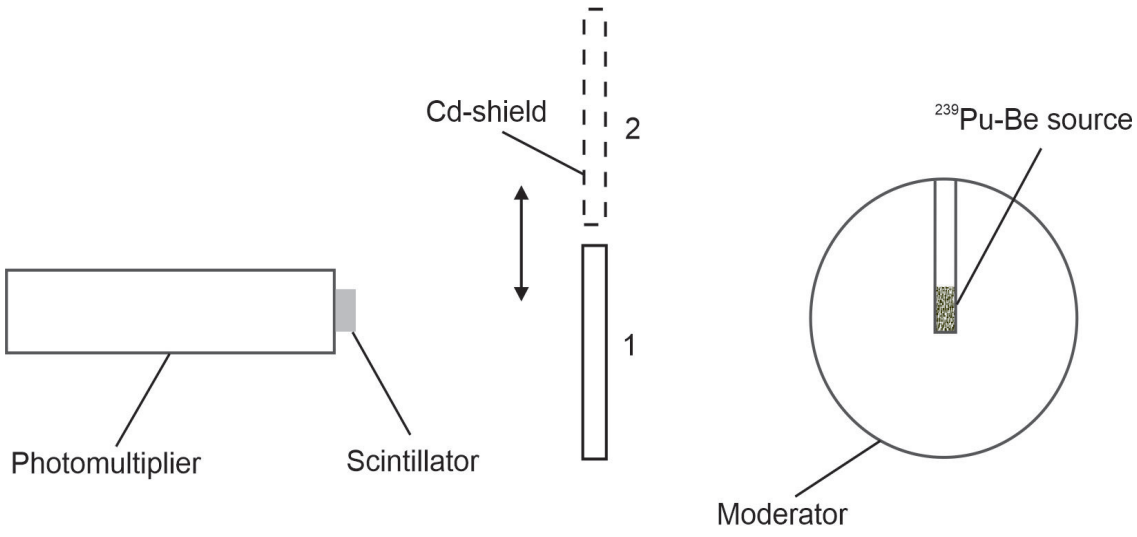

Fig. 3. Scheme for measuring the thermal neutron count rate.

count rate of thermal neutrons. Cadmium is known [31] for its significant absorption cross-section for low-energy neutrons, including thermal neutrons. However, above a certain energy threshold (E_{th}= 0.5 eV), the absorption cross-section decreases sharply, allowing only epithermal neutrons to pass through the cadmium screen. Using a cadmium screen as a filter and measuring the pulse-height spectra with and without a Cd screen, the response of a scintillator to thermal neutrons can be determined. The difference in the pulse-height spectra is called the "cadmium difference" which corresponds to the count rate of thermal neutrons.

The count rates were measured using the following technique. The count rate was determined separately for cases with and without a Cd screen. The location of the source relative to the sample under study remained unchanged. The difference between the count rates ("cadmium difference") corresponded to the count rate of thermal neutrons. The ratio of the "cadmium difference" value to the calculated count rate for thermal neutron flux passing through the input window of the detector is just the detection efficiency of thermal neutrons. Fig. 2 shows the measurement scheme.

3. Results and discussion

Table 2 presents the average grain sizes of the ^{6}LiF and ZnS(Ag) powder fractions used for obtaining nine ^{6}LiF/ZnS(Ag) samples, and their characteristics: the relative light yield and the thermal neutron detection efficiency.

According to the data of Tables 1 and 2, the range of an α-particle in ^{6}LiF significantly exceeds the average grain size of ^{6}LiF in the studied samples. This means that the α-particle will leave the ^{6}LiF converter with significant energy to be lost in ZnS(Ag) with a high enough probability, since the average grain size is comparable to the range of the α-particle in this material.

The data Table 2 demonstrate that when the ratioo of average grain sizes of ZnS(Ag) to ^{6}LiF within the range (8.8-12.8), the relative light yield and registration efficiency are higher, respectively, by (28.9-31.8)% and (29.3-32 .2)% than beyond these values. The results obtained were analyzed in more detail from the positions outlined in [24]. To do this, the ratio of the number of the LiF converter grains to the number of the ZnS(Ag) scintillator grains in each sample was determined. All samples of ^{6}LiF/ZnS(Ag) composite have the same mass ratio of the converter ^{6}LiF and scintillator ZnS(Ag), which is 1:4. The densities of LiF and ZnS are known to be 2.64 and 4.09 g/cm^3, respectively. Therefore, the LiF and ZnS volume ratio is 0.349:0.978, respectively. To simplify calculations, the ^{6}LiF and ZnS(Ag) volumes in ^{6}LiF/ZnS(Ag) samples are assumed to be 379 and 978 μm^3, respectively. For each of these samples, the following were calculated:

Table 2. Performance characteristics of the ^{6}LiF/ZnS(Ag) samples with different average grain sizes of the ^{6}LiF converter and the ZnS(Ag) scintillator.

ID	The average grain size d, μm		The size ratio of ZnS(Ag) and ^{6}LiF $d_{ZnS(Ag)}/d_{LiF}$	Performance characteristics of the 6LiF/ZnS(Ag) samples			
	ZnS(Ag)	^{6}LiF		The relative light yield L, (^{241}Am), channel number	Normalized difference in light yield , $(L-L_{min})/L_{min}$,%	The detection efficiency η, %, (^{239}Pu-Be)	Normalized difference in the detection efficiency , $(\eta-\eta_{min})/\eta_{min}$, %
1	8.0	0.5	16.0	490	12.3	20.3	1.5
2	7.0	0.6	11.7	610	29.5	28.8	30.6
3	8.0	0.7	11.4	630	31,8	29.5	32.2
4	9.0	0.7	12.8	605	28.9	29.0	31.0
5	7.0	0.8	8.8	625	31.2	28.9	30.8
6	9.0	0.8	11.2	610	29.5	28.3	29.3
7	10.0	0.6	16.6	460	6.5	22.4	10.7
8	7.0	0.9	7.8	440	2.0	23.3	14.1
9	4.5	2.0	2.2	430	0	20.0	0

Table 3. The calculation results for the ratios of the sizes and numbers of the ^{6}LiF and ZnS(Ag) grains in ^{6}LiF/ZnS(Ag) samples.

ID	1	2	3	4	5	6	7	8	9
ZnS(Ag) grain size, d_{ZnS}, μm	8	7	8	9	7	9	10	7	4.5
ZnS(Ag) grain volume, V_{ZnS}, μm^3	268	180	268	382	180	382	523	180	48
Number of ZnS(Ag) grains in a sample, N_{ZnS}	4	5	4	3	5	3	2	5	21
^{6}LiF grain size, d_{LiF}, μm	0.5	0.6	0.7	0.7	0.8	0.8	0.6	0.9	2
^{6}LiF grain volume, V_{LiF}, μm^3	0.065	0.113	0.180	0.180	0.268	0.268	0.113	0.382	4.187
Number of ^{6}LiF grains in a sample, N_{LiF}	5794	3353	2111	2111	1414	1414	3353	993	91
The ratio of the grain number of ^{6}LiF to that of ZnS(Ag), $\frac{N_{LiF}}{N_{ZnS}}$	1587:1	615:1	578:1	824:1	260:1	552:1	1794:1	182:1	4:1
The ratio of the grain size of ZnS(Ag) to that of LiF, $\frac{d_{ZnS}}{d_{LiF}}$	16	11.7	11.4	12.9	8.8	11.3	16.7	7.8	2.3
Detection efficiency, %	20.1	28.8	29.5	29	28.9	28.3	22.4	23.3	20

– the ^{6}LiF and ZnS(Ag) grain volume $v = \left(\frac{\pi d^3}{6}\right)$ in assuming they are spherically shaped;

– the numbers of ^{6}LiF and ZnS(Ag) grains $N_{LiF} = \frac{349}{v}$ and $N_{ZnS(Ag)} = \frac{978}{v}$;

– the ratio of the sizes of the ^{6}LiF and ZnS(Ag) grains $\left(\frac{d_{LiF}}{d_{ZnS}}\right)$

– the ratio of the numbers of ^{6}LiF and ZnS(Ag) grains $\left(\frac{N_{LiF}}{N_{ZnS}}\right)$.

Table 3 shows the calculation results.

Based on the data presented in Table 3 and Fig. 4, 5, samples 2 - 6 demonstrate the best thermal neutron detection efficiency (about 29%). The ratios of the sizes and numbers of ^{6}LiF and ZnS(Ag) grains (configuration 1 in [24]) seems to be optimal in these samples. On the other hand, the detection efficiency of samples 1 and 7 is lower (20-22%), since their configuration 2 [24] has an excess of lithium

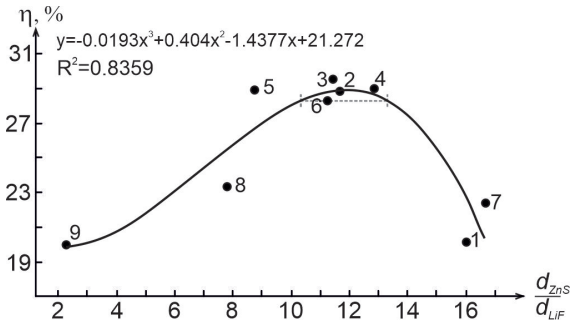

Fig. 4. The thermal neutron detection efficiency η versus the ratio of the sizes of the ZnS(Ag) and ^{6}LiF grains, $\frac{d_{ZnS}}{d_{LiF}}$. Circles are experimental data; the solid line is the regression curve. The dashed line shows the range of $\frac{d_{ZnS}}{d_{LiF}}$ values (10.3÷13.3) where the detection efficiency is η ≥ 28.3 %

grains. In this case, most of the α-particles and tritons generated in the converter are again absorbed by it, without reaching the scintillator. Samples 8 and 9, which implement configura-

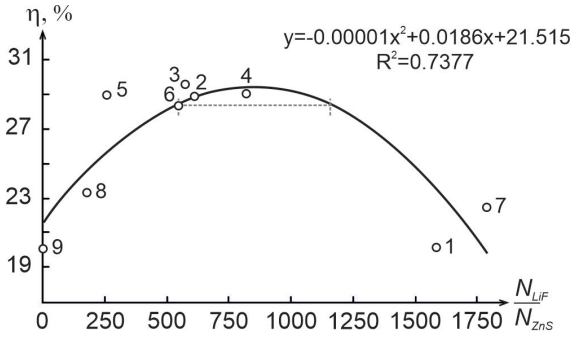

Fig.5. The thermal neutron detection efficiency η versus the ratio of the number of the ^{6}LiF and ZnS(Ag) grains, $\frac{N_{LiF}}{N_{ZnS}}$. Circles are experimental data; the solid line is the regression curve. The dashed line shows the range of $\frac{N_{LiF}}{N_{ZnS}}$ values (550÷1150), where the detection efficiency is η ≥ 28.3 %.

tion 3 [24] with a smaller number of LiF grains compared to ZnS(Ag), also exhibit low detection efficiency (20-23%) due to the reduced probability of neutron capture.

Note that these regularities take place under the assumption that each grain is spherical. However, in the practice of manufacturing composite samples, it is difficult to avoid the agglomeration of grains; this causes changes in their morphology, effective sizes and number. Disruption of the regular structure of individual grains due to their possible agglomeration is manifested in the absence of a strict correlation between the ^{6}LiF/ZnS(Ag) samples in the ratio of both the sizes and the number of ^{6}LiF and ZnS(Ag) grains. Therefore, to determine the optimal values of these ratios, it was necessary to use regression curves (solid lines in Fig. 4 and 5). The horizontal dashed line corresponding to a detection efficiency of 28.3% intersects each of these regression curves at two points. Their positions determine the ratios of the sizes $\frac{d_{LiF}}{d_{ZnS}}$ (1 to 10.3÷13.3) and the numbers $\frac{N_{LiF}}{N_{ZnS}}$ (550÷1150 to 1) of the ^{6}LiF and ZnS(Ag) grains, at which it is expected that the detection efficiency of thermal neutrons with the ^{6}LiF/ZnS(Ag) composite will reach the value close to 29%.

Undoubtedly, the thermal neutron detection efficiency of studied single-layer samples ^{6}LiF/ZnS(Ag) is relatively low and does not exceed 29.5%. Similar detection efficiency for single-layer ^{6}LiF/ZnS(Ag) samples have been reported by other authors. For example, in [22], the maximum detection efficiency of thermal neutrons is 32.4%. This was explained by the small effective thickness of the ^{6}LiF converter in a single-layer ^{6}LiF/ZnS(Ag) sample. An increase in the total thickness of the sample will lead to a sharp deterioration in its transparency and, thus, a decrease in the registration efficiency.

The scintillation response can be improved using a multilayer detector based on the ^{6}LiF/ZnS(Ag) composite with the same mass ratios of components and thicknesses of separate layers. The effective thickness of the composite scintillator is increased due to alternating its layers and organic glass plates that act as light guides.

Fig. 6 shows the schematic and general view of the ^{6}LiF/ZnS(Ag) five-layer detector made from the ^{6}LiF and ZnS(Ag) powder fractions with an average grain size of 0.7 μm and 8 μm, respectively. A composite layer of 40×25×0.2 mm^3 and a plastic plate of 40×25×3 mm^3 were used, as well as tetratex as a reflector.

Pulse-hight amplitude spectra of the ^{6}LiF/ZnS(Ag) composite detector when irradiated with a ^{239}Pu-Be neutron source represent broad distributions of the number of pulses by height

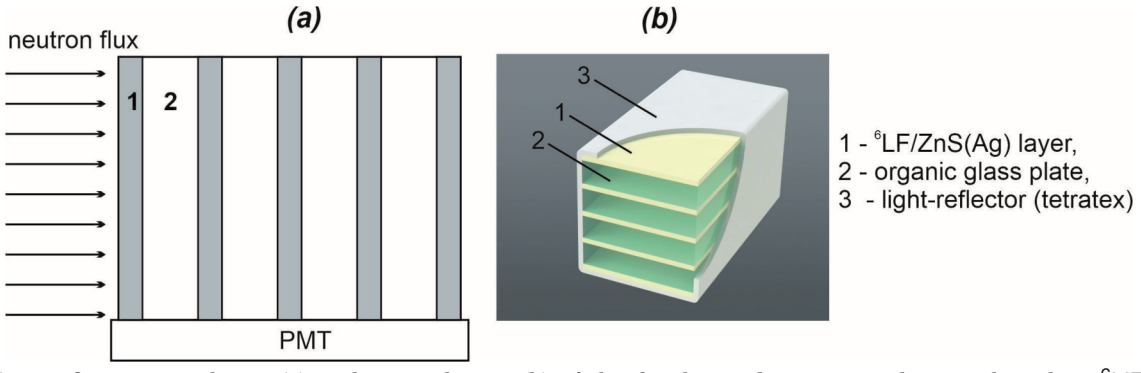

Fig. 6. Operative scheme (a) and general view (b) of the five-layered composite detector based on ^{6}LiF/ZnS(Ag).

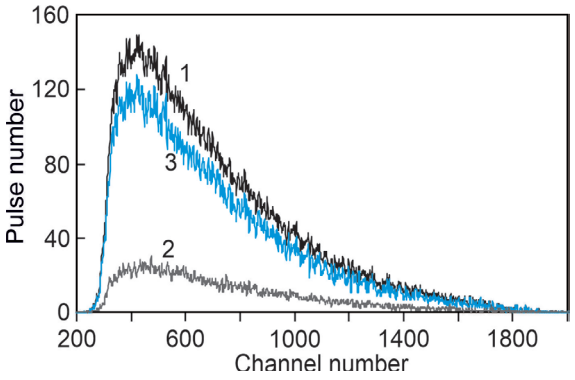

Fig. 7. Pulse-height spectra of a five-layer ^{6}LiF/ZnS(Ag) detector exposed to the neutron irradiation from ^{239}Pu-Be source: 1 – without Cd-screen, 2 – with Cd-screen, 3 – "Cd-difference".

(Fig. 7) and have a pronounced maximum; this makes it possible to reliably set the threshold for neutron detection and "cut off" noise pulses, including those associated with the detection of γ-radiation. The low spectral resolution of the detector is associated with both the spread of energy losses of charged particles in the ^{6}LiF/ZnS(Ag) scintillator and the spread of light transport to a photodetector from different places in this composite scintillator, which strongly scatters this light. A comparison of spectral distributions shows that the contribution of epithermal neutrons (2) to the total spectral distribution (1) is significantly less than the contribution of thermal neutrons (3).

The thermal neutron detection efficiency of the ^{6}LiF/ZnS(Ag) detector was determined by the cadmium difference method; this made it possible to eliminate the interaction of the detector with thermal neutrons by subtracting the pulse-height spectrum obtained with a cadmium screen from the pulse-height spectrum obtained without this screen. In this case, the area under the difference spectrum is related to the calculated number of thermal neutrons passing through the detector input window. According to the data presented in Fig. 7, the five-layer ^{6}LiF/ZnS(Ag) detector has an efficiency of 75% in detecting thermal neutrons.

It is noteworthy that the spectral distribution of pulses caused by as an exponential noise distribution is observed only at very high gains and does not contribute to the thermal neutron count rate at the specified detection threshold. This result is explained by the large "alpha-gamma ratio" of the ZnS(Ag) scintillator and the insignificant thickness (0.2 mm) of the composite layers in the used design of the ^{6}LiF/ZnS(Ag) detector.

4. Conclusions

The obtained optimal ratios of sizes (1 to 10.3÷13.3) and number (550÷1150 to 1) of grains in the ^{6}LiF converter and ZnS(Ag) scintillator provide the best values of light yield and the neutron detection efficiency (about 29%) for the one-layer composite scintillator ^{6}LiF/ZnS(Ag) with the 0.2 mm thickness and the mass component ratio of 1 ^{6}LiF:4 ZnS(Ag):2.1 binder. A decrease in the detection efficiency to 20-22% outside the optimal ratios is explained by either a deficiency or an excess of the ^{6}LiF converter grains relative to the number of ZnS(Ag) scintillator grains.

It has been shown that a multilayer scintillation detector consisting of five layers of ^{6}LiF/ZnS(Ag) composite alternating with plastic plates as light guides demonstrates a thermal neutron detection efficiency reaching 75%. Taking into account also the high selectivity of the ^{6}LiF/ZnS(Ag) scintillator to the type of radiation, it can be concluded that the thermal neutron detector based on ^{6}LiF/ZnS(Ag) is a suitable replacement for a ^{3}He counter.

References

1. G. F. Knoll, Radiation Detection and Measurement, Wiley & Sons, New York (2000).
2. P. Peerani, A. Tomanin, S. Pozzi et. al., *Nucl. Instr. and Meth.* A, **696**, 110 (2012).
3. R.T. Kouzes, A.T. Lintereur, E.R. Siciliano, *Nucl. Instr. and Meth.* A, **784**, 172 (2015).
4. T. Brückel. Applications of Neutron Scattering - an Overview. Forschungszentrum Jülich GmbH, Germany (2012).
5. S. C. Vogel, Hindawi Publishing Corporation ISRN Materials Science, Article ID 302408, 24 pages (2013).
6. R. H. Bossi, High Speed Motion Neutron Radiography. Ph.D. Thesis, Oregon State University (1976).
7. J. Rhodes, M.W. Johnson, in: Proc. Int. Conf. on Inorg. Scintillators and their Applications "SCINT'95", Delft, The Netherlands (1996), p. 73.
8. C.W.E. van Eijk, A. Bessiere, P. Dorenbos, *Nucl. Instr. and Meth.* A, **529**, 260 (2004).
9. T. Kojima, M. Katagiri, N. Tsutsui et al., *Nucl. Instr. and Meth.* A, **529**, 325 (2004).
10. C.W.E. van Eijk, *Nucl. Instr. and Meth.* A, **460**, 1 (2001).
11. A. Massara, S. Amaducci, L. Cosentino et al., *Instruments*, **7**, 1 (2023).

12. Y. Morishita, S. Yamamoto, K. Izaki at al., *Nucl. Instr. and Meth.* A, **764**, 383 (2014).
13. J. McCloy, M. Bliss, B. Miller et al., *J. Lumin.*, **57**, 416 (2015).
14. P. Dorenbos, Nucl. *Instr. and Meth*. A, **486**, 208 (2002).
15. A. R. Spowart, *Nucl. Instr. and Meth.*, **75**, 35 (1969).
16. S. K. Lee, S. Y. Kang, *Progress in Nuclear science and technology*, **1**, 194 (2011).
17. R. Stedman, *Review of Scientific Instruments*, **31**, 1156, (1960).
18. T. Tojo, *Nucl. Instr. and Meth.*, **53**, 163 (1967).
19. S.E. Mann, E.M. Schooneveld, N.J. Rhodes et. al., *Optical Materials:* X, **17**, 100226 (2023).
20. K. Era, S. Shionoya, Ya. Washizawa, *J. Phys. Chem.*, **29**, 1827 (1968).
21. S. Yamamoto, H. Tomita, *Appl. Radiat. Isot.* **168**, 109527 (2021).
22. C. Wu, B.Tang , Z.J. Sun et al., *Rad. Measur.*, **58**, 128 (2013).
23. P.J. Dean, *Progress in Solid State Chemistry*, **8**, 1 (1973).
24. A. Osovizky, K. Pritchard, J. Ziegler et al., *IEEE Trans. Nucl. Sci.*, **65**, 1025 (2018).
25. S. P. Wang, C. G. Shull, W. C. Phillips, *Rev. Sci. Instrum.*, **33**, 126 (1962).
26. Y. Yehuda-Zada, K. Pritchard, J.B. Ziegler et al., *Nucl. Instr. and Meth*. A, **892**, 59 (2018).
27. J.F. Ziegler, J. P. Biersack, M. D. Ziegler, SRIM - The Stopping and Range of Ions in Matter, SRIM Company, USA (2008).
28. J. Schelten, M. Balzhäuser, F. Höngesberg et al., *Physica B*, **234-236**, 1084 (1997). https://s100.copyright.com/AppDispatchServlet?publisherName=ELS&contentID=S0921452697000240&orderBeanReset=true
29. F. Mantler-Niderstatter, F. Bensch, F. Grass, *Instr. and Meth.*, **142**, 463 (1977).
30. A. C. Stephan, S. Dai, S.A. Wallace et al., *Radiation Protection Dosimetry* **116**, 165 (2005).
31. B. D'Mellow, D. J. Thomas, M. J. Joyce et al., *Nucl. Instr. and Meth*. A, **577**, 690 (2007).